Road Adhesion Coefficient Estimation Based on Adaptive Unscented Kalman Filter

Yi Wang, Zhen Chang, Ying Cai, Yanling Shang, Fangzheng Gao, and Jiacai Huang

Abstract—**The road adhesion coefficient is significant in vehicle safety control systems. The road adhesion coefficient plays a key role in vehicle safety systems. To estimate this parameter, this paper formulates a seven-degree-of-freedom vehicle dynamics model. The normalization of tire force is achieved by integrating the Dugoff tire model. Based on this, an adaptive unscented Kalman filter (AUKF) algorithm is proposed. To reduce the 'non-local effect' in the sampling process, a proportional correction coefficient is used in the unbiased transformation. Additionally, an adaptive coefficient is incorporated into the standard unscented Kalman filter (UKF), and the updated covariance matrix is utilized to dynamically regulate the filtering gain. This enhancement significantly improves the algorithm's adaptability to the evolving states. Joint simulations of various road conditions are conducted using Carsim and Simulink. Experimental results indicate that the proposed adaptive unscented Kalman filter algorithm can reduce computational complexity and improve convergence speed while maintaining algorithm accuracy.**

***Index Terms*—vehicle safety system, road adhesion coefficient estimation, unscented Kalman filter, unbiased transformation**

I. Introduction

With fast improvements in intelligent vehicle technologies, it becomes more and more important to estimate the road adhesion coefficient is very important. Precise estimation of this coefficient can mitigate tire wear, enhance vehicle stability, and reduce the likelihood of vehicular accidents [1]. The methodologies for estimating the road adhesion coefficient can be broadly categorized into cause-based and effect-based approaches. Cause-based methodologies rely on direct measurements obtained through various equipment and sensors for monitoring and recording both road and vehicle operational conditions, thus offering real-time insights. However, these methods are limited by notable drawbacks, including high costs and a heavy reliance on specialized equipment.

In contrast, effect-based methodologies deduce the road adhesion coefficient by analyzing the dynamic responses of the vehicle to avoid direct measurements [2-4], which demonstrate efficacy in cost reduction without compromising estimation accuracy. Recently, Ref. [5] proposed an estimator for road surface adhesion coefficient by integrating the Extended State Observer (ESO) and Adaptive Kalman Filter (AKF) algorithms. This method uses piecewise identification techniques and evaluation metrics to estimate the road surface adhesion coefficient accurately, making the process simpler and more efficient. Even though efforts are made to make the computation simpler and more efficient, delays can still happen, especially when road conditions change quickly. Ref. [6] developed an LMI-constrained UKF for accurate state estimation of unmanned vehicles under nonlinear conditions. This filter addresses the limitations of traditional Kalman filters by framing the state estimation as an optimization problem. The instability of traditional neural network weight updates can lead to low precision in estimating road surface adhesion coefficients. Ref. [7] proposed a method for estimating road surface adhesion coefficients based on Particle Swarm Optimization (PSO)-Elman neural networks. This estimation method incorporates the PSO algorithm into the Elman neural network model to reduce training absolute errors. Additionally, a linear weight decay strategy is employed to balance the weight changes in the PSO algorithm, enhancing both global and local search capabilities of particles to optimize the network weight matrix. This method makes the estimation of the road surface adhesion coefficient more precise. Ref. [8] argued that existing methods for estimating road surface adhesion coefficients have not fully leveraged the advantages of integrating image recognition and dynamic models. To Address the limited applicability of traditional estimation methods, they proposed a road surface adhesion coefficient estimation method based on the fusion of image recognition and dynamics. Ref. [9] primarily investigated the problem of trajectory tracking for vehicles under variable-speed steering and varying road surface adhesion coefficients. In their road surface adhesion coefficient estimation module, they utilized a genetic algorithm (GA) to optimize a BP neural network model. The estimation results were then transmitted as variables related to tire slip angle constraints to an MPC controller. This approach, employing

Manuscript received May 8, 2024; revised September 1, 2024. This work was partially supported by the National Natural Science Foundation of China under grant 61873120, the National Natural Science Foundation of Jiangsu Province under grant BE2021016-5, the Postgraduate Research & Practice In-novation Program of Jiangsu Province under Grant SJCX 23_1181 and the Qing Lan project of Jiangsu Province.

Yi Wang is a postgraduate student in the School of Automation, Nanjing Institute of Technology, Nanjing 211167, China (email: y00450220120@njit.edu.cn).

Zhen Chang is a postgraduate student in the School of Automation, Nanjing Institute of Technology, Nanjing 211167, China (email: y00450220449@njit.edu.cn).

Ying Cai is a postgraduate student in the School of Automation, Nanjing Institute of Technology, Nanjing 211167, China (email: y00450220407@njit.edu.cn).

Yanling Shang is an associate professor in the School of Automation, Nanjing Institute of Technology, Nanjing 211167, China (corresponding author, e-mail: hnnhsyl@126.com).

Fangzheng Gao is a professor in the School of Automation, Nanjing Institute of Technology, Nanjing 211167, China (e-mail: gaofz@126.com).

Jiacai Huang is a professor in the School of Automation, Nanjing Institute of Technology, Nanjing 211167, China (e-mail: huangjiacai@126.com)

the GA-BP neural network optimized road surface adhesion coefficient estimation method, demonstrated high estimation accuracy. However, BP neural networks also have drawbacks. Typically, the optimal number of hidden layer nodes in a BP neural network cannot be explicitly calculated by formula during network topology design, potentially leading to the training process getting stuck in local minima. Ref. [10] addressed the challenge of enhancing the control effectiveness of the Traction Control System (TCS) in automobiles, specifically focusing on improving acceleration performance while ensuring driving stability. In the process of estimating road surface adhesion coefficients, they introduced fuzzy control and decay memory filtering into the Unscented Kalman Filter (UKF). They designed an Unscented Kalman Filter estimation algorithm based on fuzzy forgetting factors to improve the tracking performance of the filtering algorithm. However, the inclusion of fuzzy control and decay memory filtering led to an increase in the computational complexity of the UKF, resulting in longer convergence times.

In response to the aforementioned questions, this study constructs a comprehensive seven-degree-of-freedom vehicle dynamics mode [11], integrating the Dugoff tire model alongside formulas for calculating normalized tire forces. Extending this groundwork, an adaptive Unscented Kalman Filter (AUKF) algorithm is introduced. During the unscented transformation phase, a proportional correction coefficient is introduced to mitigate “non-local effects” inherent in the sampling process [12]. With the conventional UKF framework, an adaptive coefficient is integrated to dynamically regulate the filter gain utilizing the updated covariance matrix, thereby augmenting the algorithm's capacity to accommodate sudden state transitions [13]. Simulation outcomes demonstrate that in comparison to the conventional UKF approach, the AUKF algorithm showcases enhanced filtering performance, characterized by swifter convergence and heightened accuracy.

This paper is organized in the following way. Section II gives the mathematical descriptions of tire and vehicle dynamics models. Section III mainly presents the improved AUKF algorithm. Section IV shows simulation results. Finally, Section V makes a summary of the main findings.

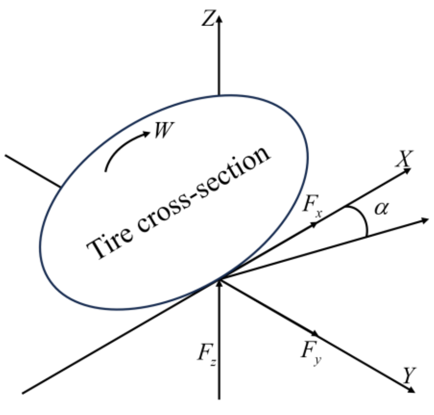

Fig. 1. Dugoff tire model

II. Tire and Vehicle Dynamics Models

A. Dugoff tire model

As a staple in automobile tire modeling, the Dugoff model primarily addresses slip rate and stiffness while disregarding factors such as radial deformation, yaw angle, and wheel speed in the computation of normalized tire force [14]. In contrast to the more intricate magic tire model, the Dugoff tire model demands fewer parameters and involves less computation. Fig. 1 is given to illustrate the force analysis conducted within the Dugoff tire model.

The expressions for longitudinal force and lateral force of the tire can be delineated in (1) and (2):

$$F_x = \mu \cdot F_z \cdot C_x \cdot \frac{\lambda}{1-\lambda} \cdot f(L) \tag{1}$$

$$F_y = \mu \cdot F_z \bullet C_y \bullet \frac{\tan(\alpha)}{1-\lambda} \bullet f(L) \tag{2}$$

where F_x is the longitudinal force of the tire, F_y is the lateral force of the tire, μ is the road adhesion coefficient, α is the side deflection angle of the tire, and C_x , C_y are the longitudinal and lateral stiffness of the tire.

$$f(L) = \begin{cases} L(2-L), L<0 \\ 1, L \geqslant 0 \end{cases} \tag{3}$$

$$L = \frac{(1-\lambda)\left(1-\varepsilon v_x \sqrt{C_x^2 \lambda^2 + C_y^2 \tan^2 \alpha}\right)}{2\sqrt{C_x^2 \lambda + C_y^2 \tan^2 \alpha}} \tag{4}$$

where ε is the speed influence coefficient and L is the boundary value, which is used to describe the nonlinear characteristics caused by the slip rate. A new Dugoff tire model formula can be obtained by normalization of the above formula:

$$F_x = \mu \cdot F_x^0 = \mu \cdot F_z \bullet C_x \bullet \frac{\lambda}{1-\lambda} \bullet f(L) \tag{5}$$

$$F_y = \mu \cdot F_y^0 = \mu \cdot F_z \cdot C_y \cdot \frac{\tan(\alpha)}{1-\lambda} \cdot f(L) \tag{6}$$

where F_x^0 and F_y^0 represent the normalized representation of the longitudinal and lateral forces of the tire respectively, and the influence of the road adhesion coefficient can be ignored.

The normalized force of the tire can be solved by the following formula:

$$F_{zFL} = m \cdot g \cdot \frac{b}{2l} - m \cdot a_x \cdot \frac{h_g}{2l} + m \cdot a_x \cdot \frac{h_g}{T_f} \cdot \frac{b}{l} \tag{7}$$

$$F_{zFR} = m \cdot g \cdot \frac{b}{2l} - m \cdot a_x \cdot \frac{h_g}{2l} + m \cdot a_x \cdot \frac{h_g}{T_f} \cdot \frac{b}{l} \tag{8}$$

$$F_{zRL} = m \cdot g \cdot \frac{b}{2l} - m \cdot a_x \cdot \frac{h_g}{2l} + m \cdot a_x \cdot \frac{h_g}{T_r} \cdot \frac{a}{l} \tag{9}$$

$$F_{zRR} = m \cdot g \cdot \frac{b}{2l} - m \cdot a_x \cdot \frac{h_g}{2l} + m \cdot a_x \cdot \frac{h_g}{T_r} \tag{10}$$

During vehicle operation, the formula for computing the slip rate is given by:

$$\lambda_{ij} = \frac{\omega_{ij} \cdot R_w - v_{ij}}{v_{ij}} \tag{11}$$

where v_{ij} is the longitudinal speed of each wheel, ω_{ij} is the angular speed of each wheel, R_w is the effective rolling radius of the wheel. The calculation formula of the wheel center speed is:

$$\begin{cases} v_{\text{cFL}} = (v_x + B_{\text{f}}\dot{\omega}_{FL}/2)\cos\delta + (v_y + L_{\text{f}}\dot{\omega}_{FL})\sin\delta \\ v_{\text{cFR}} = (v_x - B_{\text{f}}\dot{\omega}_{FR}/2)\cos\delta + (v_y + L_{\text{fl}}\dot{\omega}_{FR})\sin\delta \\ v_{\text{cRL}} = v_x + B_{\text{f}}\dot{\omega}_{RL}/2 \\ v_{\text{cRR}} = v_x - B_{\text{f}}\dot{\omega}_{RR}/2 \end{cases} \tag{12}$$

where v_{cFL}, v_{cFR}, v_{cRL} and v_{cRR} are the speeds at the center of the left front wheel, right front wheel, left rear wheel and right rear wheel; ω_{FL}, ω_{FR}, ω_{RL} and ω_{RR} are the angular velocities of the left front wheel, right front wheel, left rear wheel and right rear wheel, respectively. v_x is the longitudinal speed of the car and v_y is the lateral speed of the car.

The formula for calculating the tire's side deflection angle is expressed as follows:

$$\begin{cases} \alpha_{FL} = -\delta + \arctan\dfrac{v_y + L_f\dot{\omega}_{FL}}{v_x + B_f\dot{\omega}_{FL}/2} \\ \alpha_{FR} = -\delta + \arctan\dfrac{v_y + L_f\dot{\omega}_{FR}}{v_x - B_f\dot{\omega}_{FR}/2} \\ \alpha_{RL} = \arctan\dfrac{v_y - L_f\dot{\omega}_{RL}}{v_x + B_f\dot{\omega}_{RL}/2} \\ \alpha_{RR} = \arctan\dfrac{v_y - L_f\dot{\omega}_{RR}}{v_x - B_f\dot{\omega}_{RR}/2} \end{cases} \tag{13}$$

B. *Vehicle dynamics model*

Since the longitudinal, lateral, and yaw motions of the vehicle is imperative for accurately estimating both the motion state parameters and the road adhesion coefficient [15], the state of the tire directly influences the road adhesion coefficient. Thus, taking the inclusion of the rotation of all four wheels into consideration. this paper adopts the seven degree of freedom model as the dynamic model, as illustrated in Fig. 2. The vehicle's center of mass is the starting point for the coordinate system in this model. The vertical axis aligns with the forward direction of the vehicle, with forward motion designated as positive. The horizontal axis corresponds to the vehicle's lateral direction, with leftward movement denoted as positive. Furthermore, torque within the horizontal plane is deemed positive in the counterclockwise direction. For the simulation, the vehicle dynamics model assumes several things: no aerodynamic effects, no vertical movement, no pitch and roll motions, and all tires have the same physical properties. model are as follows:

Longitudinal movement:

$$\dot{v}_x = a_x + v_y \cdot \gamma \tag{14}$$

$$a_x = \frac{1}{m}(F_{xFL}cos\delta + F_{xFR}cos\delta + F_{xRL} + F_{xRR} \\ -F_{yFL}sin\delta - F_{yFR}sin\delta) \tag{15}$$

Lateral movement:

$$\dot{v}_y = a_y - v_x \cdot \gamma \tag{16}$$

$$a_y = \frac{1}{m}(F_{xFL}sin\delta + F_{xFR}sin\delta + F_{yFL}cos\delta + \\ F_{yFR}cos\delta + F_{yRL} + F_{yRR}) \tag{17}$$

Yaw movement:

$$\dot{\gamma} = \frac{1}{I_z} \cdot \Gamma \tag{18}$$

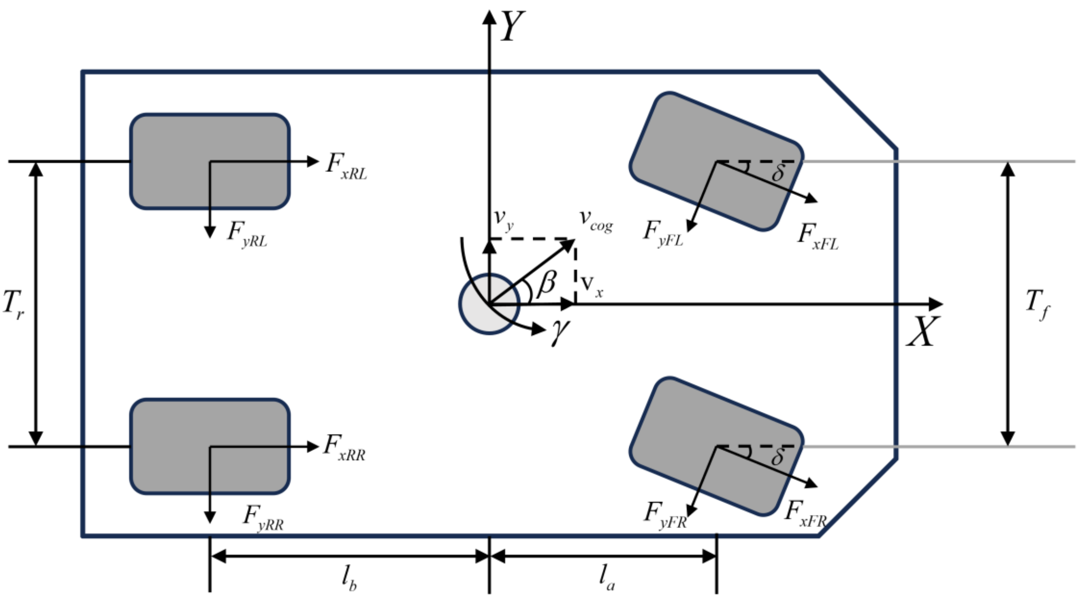

Fig. 2. Seven degree of freedom vehicle dynamics model

$$\begin{aligned}\Gamma &= l_a(F_{xFL}+F_{xFR})sin\delta + l_a(F_{xFL}+F_{yFR})cos\delta \\ &-l_b(F_{yRL}+F_{yRR}) - \frac{t_f}{2}(F_{xFL}-F_{xFR})cos\delta \\ &+\frac{t_f}{2}(F_{yFL}-F_{yFR})sin\delta - \frac{t_r}{2}(F_{xRL}-F_{xRR})\end{aligned} \quad (19)$$

Wheel rotation equation:

$$\begin{aligned} J\dot{w}_{FL,FR} &= T_{dFL,FR} - T_{bFL,FR} - F_{xFL,FR}R \\ J\dot{w}_{RL,RR} &= F_{xRL,RR}R - T_{bRL,RR}\end{aligned} \quad (20)$$

where a_x and a_y are longitudinal and lateral acceleration respectively, γ is the yaw speed of the vehicle, δ is the angle of the front wheel of the vehicle, m is the mass of the vehicle, the inertia of the vehicle rotating around the Z axis is denoting I_z, and the yaw moment of the vehicle around the Z axis is denoting Γ. J is the rotational inertia of the wheel and R is the rolling radius of the tire. Subscripts *FL*, *FR*, *RL* and *RR* represent the left front, left rear, right front and right rear wheels respectively, then F_{xi} and F_{yi} represent the longitudinal and lateral forces on the corresponding tires respectively, $\dot{w}_i$ represents the angular acceleration of the corresponding wheels, T_d and T_b represent the driving torque and braking torque of the corresponding wheels respectively.

III. Road Adhesion Coefficient Estimation

A. Estimation of road adhesion coefficient based on AUFK

(1) Improved unbiased transformation

The unbiased transformation is a key part of the standard Unscented Kalman Filter (UKF) method, especially good for solving nonlinear problems [16]. Initially, Sigma points are meticulously chosen to approximate the statistical characteristics of the original state. Subsequently, nonlinear transformations are applied to these points, yielding the statistical properties of the transformed state. Ultimately, the mean and covariance of these transformed points are judiciously weighted to yield the optimal estimation of the nonlinear problem.

The nonlinear system in this paper can be represented by $y = f(x)$, assuming that $\bar{x}$ and P_x are the mean and variance of the state vector x, respectively. To satisfy the statistical characteristics of calculating y, a Sigma vector χ_i, $i = 2L+1$ is first set, and then weighted to obtain the corresponding mean and covariance weights $W_i^{(m)}$ and $W_i^{(c)}$. Where L is the number of Sigma points of the sampling strategy. The UT transformation process for the symmetric sampling strategy is as follows:

$$\chi_0 = \bar{x}, i = 0 \quad (21)$$

$$\chi_i = \begin{cases} \bar{x} + \left(\sqrt{(L+\lambda)P_x}\right)_i, i = 1,2\ldots,L \\ \bar{x} + \left(\sqrt{(L+\lambda)P_x}\right)_{i-L.}, i = L+1, L+2\ldots,2L \end{cases} \quad (22)$$

$$W_0^{(m)} = \lambda/(L+\lambda) \quad (23)$$

$$W_0^{(c)} = \lambda/(L+\lambda) + (1-\alpha^2+\beta) \quad (24)$$

$$W_i^{(m)} = W_i^{(c)} = 1/[2(L+\lambda)], i = 1,2,\ldots,2L \quad (25)$$

$$\lambda = \alpha^2(L+\kappa) - L \quad (26)$$

where λ is a scale parameter, α is used to calculate the distribution range of Sigma points near x, κ is a second-order scale parameter, β is the combination of previous states related to x distribution, and $(\sqrt{(L+\lambda)P_x})_i$ represents the value of the i row of the square root of the matrix.

However, in this UKF algorithm, the distance between the Sigma point and the mean point $\sqrt{(L+\lambda)P}$ grows as the dimension grows, which causes a 'non-local effect' during sampling [17]. The measurement function's nonlinearity directly impacts the filtering accuracy of the algorithm. In order to solve this "non-local effect" and ensure the semi-positive quality of the covariance matrix, this paper considers the proportional sampling correction of the Sigma point set obtained previously. The revised formula is as follows:

$$\begin{cases} X^{(i)}(k|k) = X^{(0)} + a_1 \times (X^{(i)} - X^{(0)}), i = 1,\cdots,2n \\ X^{(i)}(k+1|k) = f(k, X^{(i)}(k,k)), i = 1,\cdots,2n \end{cases} \quad (27)$$

where a_1 is the scaling correction parameter, and its value is $[0,1]$, $X^{(i)}(k+1|k)$ is the one-step prediction of Sigma point set, and f is the nonlinear transformation of the system state quantity.

Put the assumed Sigma points into the nonlinear relation $f(\cdot)$ to obtain the transformed Sigma point set $\{y_i\}$:

$$y_i = f(\chi_i), i = 0,1,2...,2L \quad (28)$$

Then the transformed Sigma points are weighted to estimate the mean and variance of the y approximation.

$$\begin{aligned} \bar{y} &\approx \sum_{i=0}^{2L} W_i^{(m)} y_i \\ P_{yy} &= \sum_{i=0}^{2L} W_i^{(c)} \{y_i - \bar{y}\}\{y_i - \bar{y}\}^T \end{aligned} \quad (29)$$

(2) AUK filter flow

This paper proposes an AUK filter flow based on the 'modified unbiased transform:

$$\begin{cases} x_{k+1} = f(x_k, u_k, w_k) \\ y_k = h(x_k, v_k) \end{cases} \quad (30)$$

where x_k is the state variable, u_k is the input variable, y_k is the output variable, w_k and v_k are the process noise and output noise respectively.

1) Filter initialization, $k = 0$:

$$\hat{x}_0 = E[x_0] \quad (31)$$

$$P_0 = E\left[(x_0 - \hat{x}_0)(x_0 - \hat{x}_0)^T\right] \quad (32)$$

where($x(0|0)$)is the initial value of x_0.

2) For $k = 1,2,\cdots$:

(a) $2n+1$ Sigma points are obtained according to UT transformation theory:

$$\chi(k-1) = \left[\hat{x}(k-1) \pm \sqrt{(n+\lambda)P_i(k-1)}\right], i = 1,2\ldots,n \quad (33)$$

where λ is the scale parameter and n is the number of sampling points.

(b) Time update

Take the obtained Sigma point set and calculate the transformed Sigma point set through the equation of state:

$$\chi(k|\ k-1) = f\left(\chi(k-1), u(k-1)\right) \tag{34}$$

According to UT transformation theory, the mean weight is carried out to calculate the predicted mean of the state:

$$\hat{x}(k|\ k-1) = \sum_{i=0}^{2N} W_i^{(m)} \chi_i(k|\ k-1) \tag{35}$$

where $\chi_i(k|\ k-1)$ is column i of matrix $\chi(k|\ k-1)$, $i = 0,1,..\ 2N$.

According to UT transformation theory, covariance weighting is performed to calculate the predicted variance of the state:

$$\begin{aligned} P\left(k\,|\,k-1\right) = \sum_{i=0}^{2N} W_i^{(c)} (\chi_i\left(k\,|\,k-1\right) - \hat{x}(k\,|-1)) \\ \left(\chi_i\left(k|\ k-1\right) - \hat{x}\left(k\,|\,k-1\right)\right)^T + Q_k \end{aligned} \tag{36}$$

Bring the transformed Sigma point into the observed equation for nonlinear analysis:

$$\xi\left(k|\ k-1\right) = h\left(\chi(k-1)\right) \tag{37}$$

Then the weighted summation method is used to estimate the predicted values of the observed variables:

$$\hat{y}(k|\ k-1) = \sum_{i=0}^{2N} W_i^{(m)} \xi_i(k|\ k-1) \tag{38}$$

where $\xi_i(k|\ k-1)$ is column i of matrix, $i = 0,1,\ldots,2N$.

(c) Measurement updates

Within the UT transformation, a proportional correction coefficient is incorporated to mitigate the "non-local effect" encountered during the sampling process. While this correction proves efficacious, practical implementation reveals that the UKF algorithm is highly sensitive to initial filter values, potentially leading to filter divergence [18]. Hence, this study introduces a noise adaptive coefficient to enhance the original algorithm by augmenting the proportional correction. This noise adaptive coefficient estimates and corrects noise and statistical parameters of uncertain system models. It also adjusts predicted values based on observations. Consequently, the traditional forecast covariance undergoes the following update:

Calculate the updated state covariance:

$$\begin{aligned} P_{yy} = \alpha_k \sum_{i=0}^{2N} W_i^{(c)} (\zeta_i\left(k\,|\,k-1\right) - \hat{y}(k|\ k-1)) \\ \left(\zeta_i\left(k|\ k-1\right) - \hat{y}\left(k\,|\,k-1\right)\right)^T + R_k \end{aligned} \tag{39}$$

Calculate the cross-correlation matrix:

$$\begin{aligned} P_{xy}\left(k\,|\,k-1\right) = \alpha_k \sum_{i=0}^{2N} W_i^{(c)} \left(\chi_i\left(k\,|\,k-1\right) - \hat{x}(k|\ k-1)\right) \\ \left(\chi_i\left(k|\ k-1\right) - \hat{y}\left(k\,|\,k-1\right)\right)^T \end{aligned} \tag{40}$$

where α_k is the noise adaptive coefficient, and the value range is $0 < \alpha_k \leq 1$.

Choosing the right adaptive coefficient is crucial. It balances the weight between the estimated and observed values and reduces the impact of interference on the results. The value of α_k is as follows:

$$\alpha_k = \begin{cases} 1, trace(\mathbf{m}_k \mathbf{m}_k^T) \leqslant trace(\mathbf{P}_{yy}) \\ \dfrac{trace(\mathbf{P}_{yy})}{trace(\mathbf{m}_k \mathbf{m}_k^T)}, trace(\mathbf{m}_k \mathbf{m}_k^T) > trace(\mathbf{P}_{yy}) \end{cases} \tag{41}$$

where, the predicted residual:

$$\mathbf{m}_k = Z^{(i)}(k+1\,|\,k) - \bar{Z}(k+1\,|\,k) \tag{42}$$

Calculate the updated filter feedback gain:

$$K\left(k\right) = P_{xy}(k|\ k-1) P_{yy}^{-1} \tag{43}$$

Calculate the filter value after the status update:

$$\hat{x}(k\,|\,k) = \hat{x}(k\,|\,k-1) + K(k)(y(k) - \hat{y}(k\,|\,k-1)) \tag{44}$$

Check the difference matrix after calculating the state:

$$P\left(k\,|\,k\right) = P\left(k\,|\,k-1\right) - K\left(k\right) P_{yy} K\left(k\right)^T \tag{45}$$

(3) Road adhesion coefficient estimation model

In this study, a co-simulation approach utilizing Carsim and Simulink is employed to validate the algorithm's accuracy. Parameters such as vehicle mass, front wheel distance, and rear wheel distance are configured within the vehicle model in Carsim. Meanwhile, the Dugoff tire model, seven-degree-of-freedom vehicle dynamics model, and algorithm are implemented in Simulink. Through the integration of Carsim and Simulink, the comparative advantages of the Adaptive Unscented Kalman Filter (AUKF) in estimating pavement adhesion coefficient, in terms of convergence and estimation accuracy, are demonstrated across diverse road conditions when juxtaposed with the traditional UKF algorithm. The overarching framework of the model is illustrated in Fig. 3.

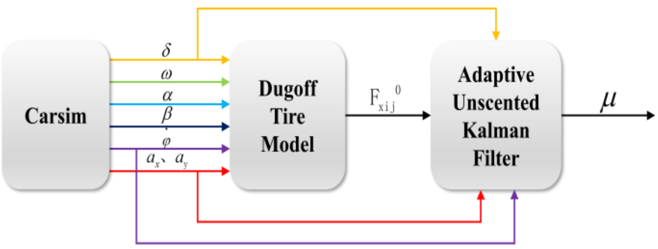

Fig. 3. Model framework

IV. Simulation Results

To evaluate the efficacy of the proposed method under actual braking scenarios, a series of experiments are meticulously designed in this study. These experiments encompass diverse road conditions, including low adhesion coefficient surfaces, high adhesion coefficient splice roads, and transitional roads. Through systematic experimentation, a comparative analysis of the performance between the UKF and AUKF algorithms is conducted.

To facilitate a comprehensive comparison, high and low adhesion coefficient conditions are concurrently simulated through splice pavement experimentation. Splice pavement entails partitioning the road into distinct sections, each assigned a specific adhesion coefficient. Specifically, when the vehicle's speed exceeds 48 km/h, the adhesion coefficient for dry cement and dry asphalt surfaces is set at 0.8, while in wet conditions, it is adjusted to 0.5. Simulation is commonly represented as depicted in the Fig. 4.

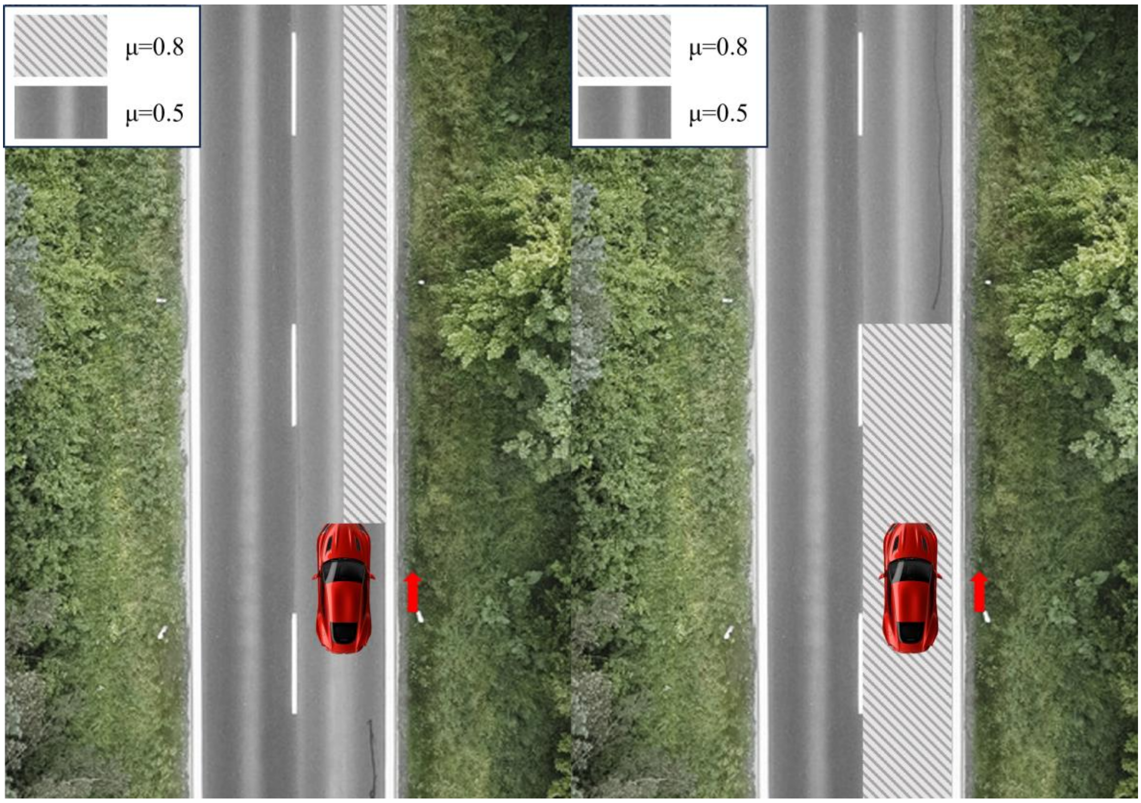

Fig. 4. Road conditions of simulation.

For simulation purposes, a dedicated vehicle model within Carsim is selected and configured based on pertinent parameters outlined in TABLE I.

TABLE I
VEHICLE PARAMETERS

argument	value
Vehicle mass (kg)	1765
Front wheel distance (m)	1.6
Rear wheel distance (m)	1.6
Distance from center of mass to front axis (m)	1.2
Distance from center of mass to rear axis (m)	1.4
Effective rolling radius of the wheel (m)	0.354
Moment of inertia (kg/m^2)	3234

(1) Low adhesion road simulation verification

For simulation verification of low adhesion road surface, the road adhesion coefficient of left front wheel and left rear wheel μ is set as 0.5, the initial vehicle speed is 16m/s, and the simulation time is 1s. The simulation results are shown from Fig. 5 to Fig. 9.

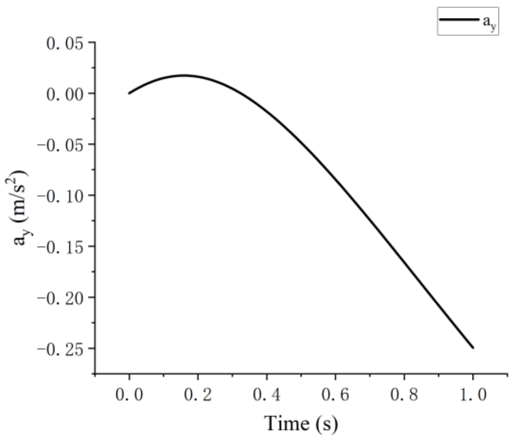

Fig. 5. Longitudinal acceleration

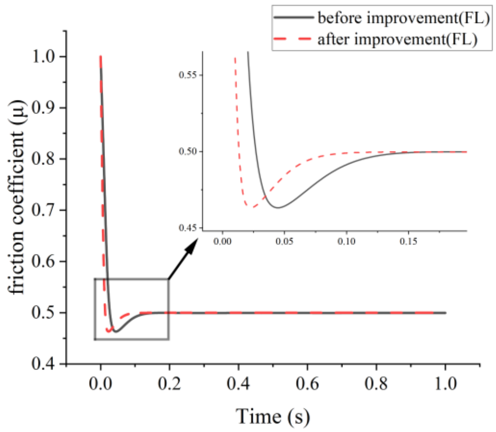

Fig. 6. Friction coefficient of the tires (FL)

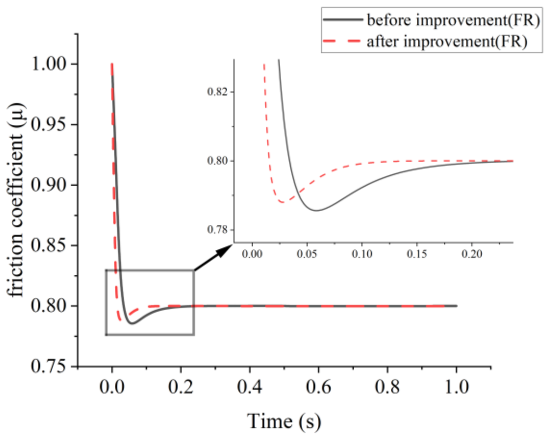

Fig. 7. Friction coefficient of the tires (FR)

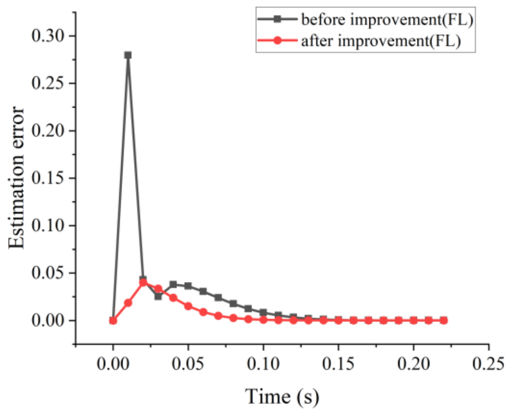

Fig. 8. Estimation error of the tires (FL)

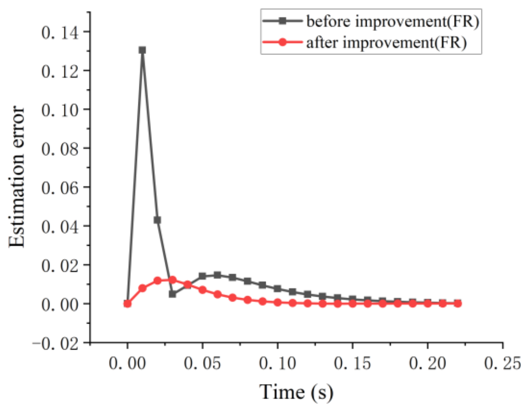

Fig. 9. Estimation error of the tires (FR)

Through analysis and comparison of simulation curves, both the AUKF and UKF algorithms demonstrate a tendency to converge towards the predefined standard value. However, the AUKF algorithm exhibits notably swifter convergence and heightened precision when juxtaposed with the UKF algorithm. Building upon the foundation of the standard UKF, this study introduces the noise adaptive coefficient to mitigate anomalous disturbances, thereby refining the estimated outcomes of the system.

In tests for estimating the road adhesion coefficient of the left front and rear wheels, the AUKF method shows much smaller errors than the UKF method, with about 2% difference.

(2) High adhesion road simulation verification

Keeping all other Carsim parameters the same, the road adhesion coefficient is set to 0.8. Then, simulations are done on the right front and rear wheels. The simulation outcomes, depicted from Fig.10 to Fig.14, emonstrate similarities to those observed on pavements with low adhesion coefficients. Notably, the convergence speed is accelerated, albeit accompanied by a modest increase in estimated error, ranging from 2% to 3%. Furthermore, the maximum estimated error experiences a significant reduction.

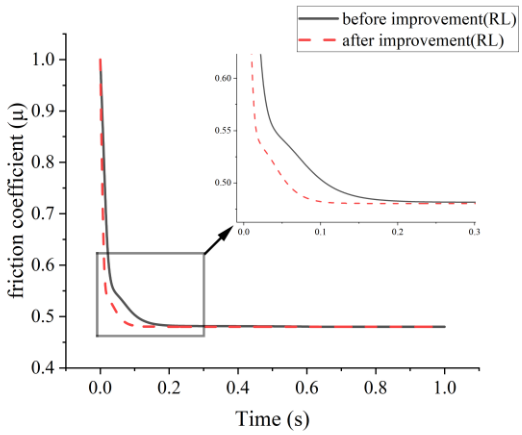

Fig. 11. Friction coefficient of the tires (RL)

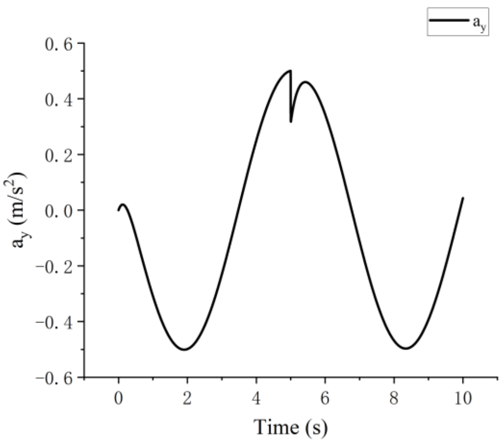

Fig. 10. Longitudinal acceleration

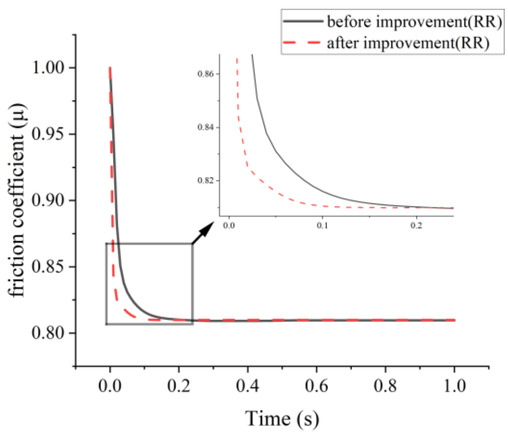

Fig. 12. Friction coefficient of the tires (RR)

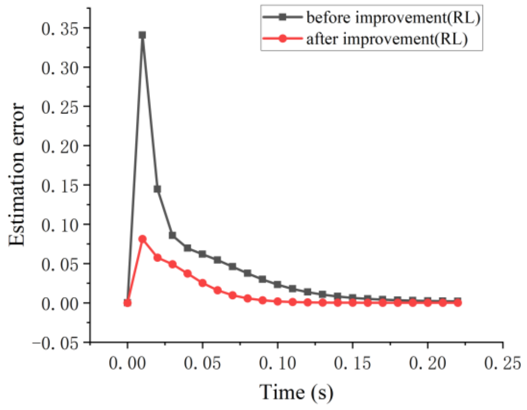

Fig. 13. Estimation error of the tires (RL)

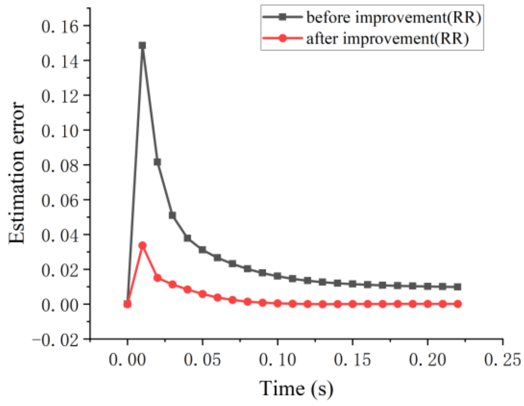

Fig. 14. Estimation error of the tires (RR)

(3) Simulation verification of transition road

To simulate the abrupt variation in road adhesion coefficient, this study establishes a scenario wherein the coefficient transitions from 0.8 to 0.5 in the 5th second, symbolizing an instance where the vehicle encounters sudden rain while in motion. Other parameter settings remain unaltered, and the simulation outcomes are illustrated from Fig. 15 to Fig. 20.

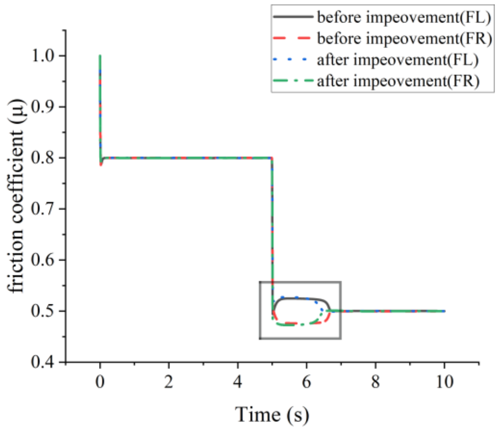

Fig. 15. Friction coefficient of tires (FL & FR)

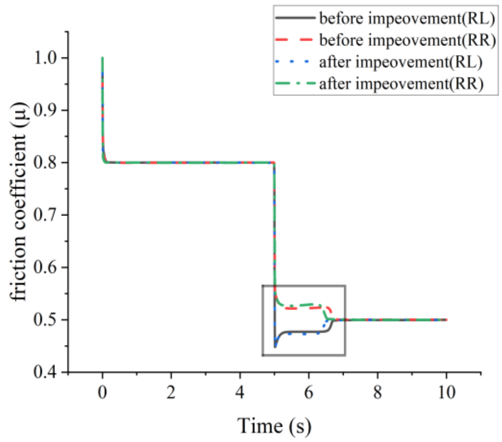

Fig. 17. Friction coefficient of tires (RL & RR)

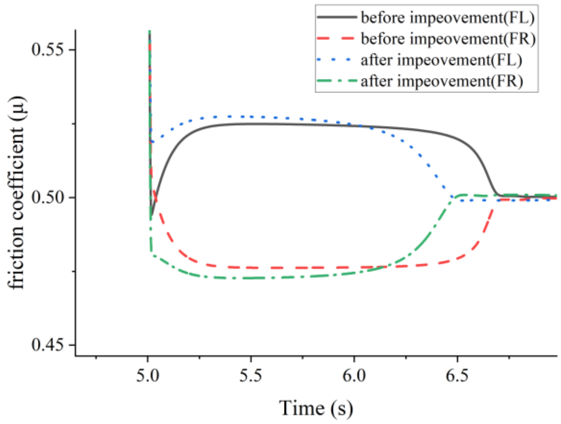

Fig. 16. Magnified view

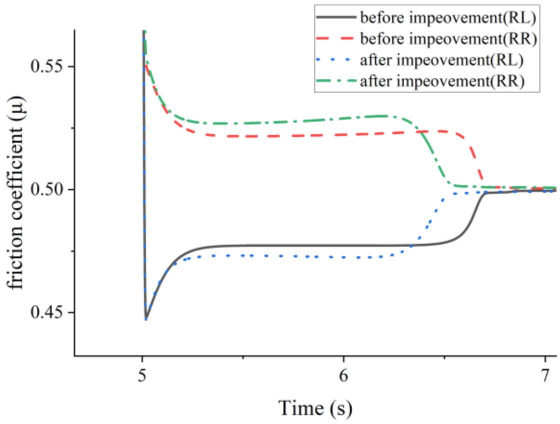

Fig. 18. Magnified view

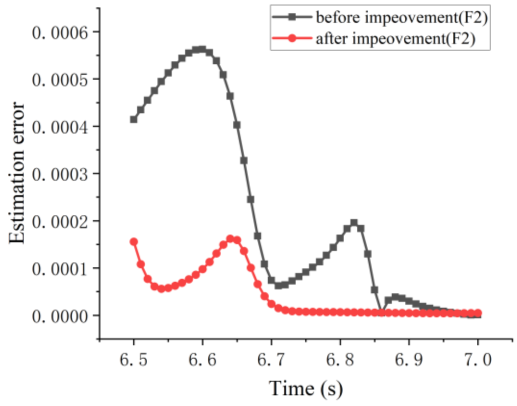

Fig. 19. Estimation error of the tires (F2)

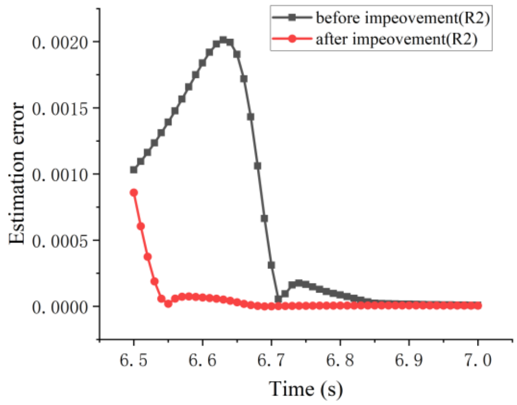

Fig. 20. Estimation error of the tires (R2)

When there are sudden changes in the road adhesion coefficient, the proposed AUKF algorithm quickly converges to the set value, with slight improvements in estimation error.

V. Conclusions

Based on by a seven-degree-of-freedom vehicle dynamics model and the Dugoff tire model, this study presents a comprehensive approach to estimate the pavement adhesion coefficient. An AUKF algorithm is proposed for this purpose. Initially, the algorithm employs a proportional correction coefficient in the unbiased transformation stage to mitigate the "non-local effect" inherent in the sampling process. Subsequently, an adaptive coefficient is integrated into the standard UKF, and the updated covariance matrix is employed to dynamically regulate filtering gain in real time, which enhances the algorithm's adaptability to abrupt states. Experimental verification corroborates the efficacy of the proposed approach, leading to the following conclusions.

(1) The proposed AUKF algorithm can achieve precision estimation of the road adhesion coefficient, effectively capturing variations across diverse road conditions.

(2) Under identical conditions, owing to the correction of the "non-local effect" and the incorporation of the adaptive coefficient in the unbiased transformation stage, the proposed AUKF outperforms the traditional UKF in terms of filtering accuracy and convergence speed.

References

[1] Zheng Zhang, Chunguang Liu, Xiaojun Ma, Yunyin Zhang, and Luming Chen, “Driving force coordinated control of an 8×8 in-wheel motor drive vehicle with tire-road friction coefficient,” *Defence Technology*, vol.18, no.1, pp.119-132, 2022.

[2] Indrazno Siradjuddin, Gilang Al Azhar, Sapto Wibowo, Ferdian Ronilaya, Cahya Rahmad, and Erfan Rohadi, “A general inverse kinematic formulation and control schemes for omnidirectional robots,” *Engineering Letters*, vol.29, no.1, pp.1344-1358, 2022.

[3] Natalia Danilova, Grigory Beliavsky, and Irina Zemlyakova, “Optimal control in binary models with the disorder,” *Engineering Letters*, vol.29, no.4, pp.1359-1364, 2021.

[4] Jun Ma, Xunhuan Ren, Liu Yuan, Viktar Yurevich Tsviatkou, and Valery Kanstantinavich Kanapelka, “An improved adaptive thinning framework,” *Engineering Letters*, vol.30, no.3, pp.1138-1145, 2022.

[5] Xinrong Zhang, Xin Wang, Xinle Gong, Jin Huang, Dan Huang and Pengxing Wang, “Segmented identification method of tire-road friction coefficient for intelligent vehicles,” *Automotive Engineering*, vol.45, no.10, pp.1923-1932, 2023.

[6] Renbo Qing, Xiaoming Tang, Hua Huang, and Yongzhen Cao, “An MPC method for trajectory tracking of unmanned vehicle with LMI-constrained unscented kalman filter,” *IAENG International Journal of Computer Science*, vol.51, no.4, pp.447-462, 2024.

[7] Juncheng Wang, and Fahui Wang, “Variable weight PSO-Elman neural network based road adhesion coefficient estimation,” *Journal of Zhejiang University (Engineering Science)*, vol.58, no.3, pp.622-634, 2024.

[8] Lei Zhang, Keren Guan, Xiaolin Ding, Pengyu Guo, Zhenpo Wang and Fengchun Sun, “Tire-road friction estimation method based on Image recognition and dynamics fusion,” *Automotive Engineering*, vol.45, no.7, pp.1222-1236, 2023.

[9] Yunfei Zha, Xiaolong Lv, Huiqin Che, Yingchun Yi and Yanyan Wang, “Vehicle trajectory tracking control based on road adhesion coefficient estimation,” *Automotive Engineering*, vol.45, no.6, pp.1010-1021, 2023.

[10] Hongbo Wang, Chunyang Wang, Han Gao, and Shihan Xu, “Vehicle traction force control based on the road adhesion coefficient estimation by FFUKF,” *Chinese Journal of Theoretical and Applied Mechanics*, vol.54, no.7, pp.1866-1879, 2022.

[11] Zhigang Zhou, Xinqing Ding, Zhichong Shi, Xiaofei Yin, and Xiangming Meng, “In-wheel motor electric vehicle based on fuzzy neural network yaw stability optimization control,” *Engineering Letters*, vol.31, no.4, pp.1717-1723, 2023.

[12] Hirofumi Miyajima, Noritaka Shigei, and Hiromi Miyajima, “Fuzzy modeling using vector quantization and local linear mapping,” *IAENG International Journal of Computer Science*, vol.47, no.4, pp.847-854, 2020.

[13] Ienkaran Arasaratnam and Simon Haykin, “Cubature kalman filters,” *IEEE Transactions on Automatic Control*, vol.54, no.6, pp.1254-1269, 2009.

[14] Weidong Liu, Zongzhi Han, Zhenhai Gao, and Yanhu Kang, “Real-time pavement recognition technology based on intelligent tire system,” *Automotive Engineering*, vol.46, no.4, pp.617-625, 2024.

[15] Yijie Chen, Yafeng Zhang, Long Xu, Fu Du, and Fen Zheng, “Dynamic modeling of high-mobility tracked vehicles and analysis of the optimization of suspension characteristics,” Scientia Sinica Technologica, vol.53, no.9, pp.1545-1555, 2023.

[16] Xiangming Meng, Zhigang Zhou, and Wenhao Yang, “Controlling yaw stability of hub motor electric vehicle based on unscented kalman filtering,” *Joumal of Highway and Transportation Research and Development*, vol.40, no.7, pp.1-16, 2024.

[17] Guanyu Zhang, Jinxin Luo, Hao Xu, Yitian Wang, Tianhao Wang, Jun Lin and Yang Liu, “An improved UKF algorithm for extracting weak signals based on RBF neural network,” IEEE Transactions on Instrumentation and Measurement, vol.71, pp.1-14, 2022.

[18] Zhaozhe Yang, Yuezhong Li, and Guangwen Wu, “IMU sensor denoising based on unscented Kalman filter and wavelet analysis,” *Modern Electronics Technique*, vol.47, no.5, pp.53-59, 2024.